SIN-CHN SCIENTIFIC PRESS PTE.LTD.

Molecular & Cellular Biomechanics 2025, 22(2), 825.
https://doi.org/10.62617/mcb825

Article

Analyzing the impact of ferroptosis on atherosclerotic plaque formation through biomechanical modeling

Ru Du, Yuhong Zuo, Xinan Wang, Jiawang Ding*

The First College of Clinical Medical Science, China Three Gorges University, Yichang 443000, China; dfng12475@163.com

CITATION

Du R, Zuo Y, Wang X, Ding J. Analyzing the impact of ferroptosis on atherosclerotic plaque formation through biomechanical modeling. Molecular & Cellular Biomechanics. 2025; 22(2): 825. https://doi.org/10.62617/mcb825

ARTICLE INFO

Received: 18 November 2024
Accepted: 25 November 2024
Available online: 11 February 2025

Abstract: Atherosclerotic plaque rupture, a primary cause of acute cardiovascular events, is fundamentally influenced by biomechanical forces. While ferroptosis, an iron-dependent form of regulated cell death, has been implicated in atherosclerosis progression, its impact on plaque biomechanics and stability remains poorly understood. We developed a comprehensive biomechanical model integrating ferroptotic parameters with plaque structural mechanics. Human carotid endarterectomy specimens (n = 45) were analyzed using a multi-modal approach combining mechanical testing, molecular analysis, and computational modeling. Plaque samples were categorized into stable (n = 15), vulnerable (n = 15), and transitional (n = 15) groups. Changes in mechanical properties, ferroptotic markers, and stress distributions were assessed over 72 h under controlled conditions. Ferroptosis induction resulted in significant alterations of plaque biomechanics. Peak circumferential stress in the fibrous cap increased from 142.3 ± 12.4 kPa to 286.4 ± 22.7 kPa ($p < 0.001$), while cap thickness decreased from 165.4 ± 12.3 μm to 98.6 ± 18.4 μm ($p < 0.001$). The iron accumulation showed a strong negative correlation with plaque stability ($r = -0.892$, $p < 0.001$). Mechanical testing revealed a 56.5% reduction in tensile strength and a 52.3% decrease in strain at failure in vulnerable plaques. Sensitivity analysis identified fibrous cap thickness (NSC = 0.924) and iron concentration (NSC = 0.856) as critical determinants of plaque stability. Our findings establish ferroptosis as a significant mediator of plaque biomechanical deterioration. The strong correlations between ferroptotic markers and mechanical instability suggest that targeting ferroptotic pathways may provide novel approaches for maintaining plaque stability. This study provides a quantitative framework for understanding the mechanical consequences of ferroptosis in atherosclerotic disease progression and identifies potential therapeutic targets for plaque stabilization.

Keywords: atherosclerosis; ferroptosis; biomechanics; plaque stability; stress analysis; iron metabolism; cardiovascular disease; mechanical modeling

1. Introduction

The pathophysiology of atherosclerotic plaque destabilization represents a critical area of cardiovascular research, as plaque rupture remains the primary trigger for acute coronary events [1–3]. Recent evidence has highlighted ferroptosis, a distinctive form of regulated cell death characterized by iron-dependent lipid peroxidation, as a potential key mediator in atherosclerotic progression [4,5]. While the traditional focus has centered on apoptotic and necrotic cell death pathways, the role of ferroptosis in plaque biomechanics and stability remains unexplored mainly [6–8]. Atherosclerotic plaques develop through a complex interplay of lipid accumulation, inflammation, and vascular remodeling [9,10]. The stability of these plaques depends critically on their structural composition, particularly the integrity of the fibrous cap and the underlying extracellular matrix [11]. Traditional understanding

has emphasized the role of matrix metalloproteinases and inflammatory processes in plaque destabilization. However, emerging evidence suggests that ferroptotic cell death may introduce unique mechanical perturbations that significantly influence plaque vulnerability [12–14].

The biochemical signature of ferroptosis, characterized by accumulated iron, depleted glutathione, and extensive lipid peroxidation, presents a distinct mechanism for tissue degradation [15,16]. These molecular events may substantially alter the mechanical properties of atherosclerotic plaques through multiple pathways. First, the iron-catalyzed formation of reactive oxygen species can directly compromise structural proteins [17]. Second, the death of smooth muscle cells, the primary producers of stabilizing extracellular matrix components, may weaken the plaque's mechanical integrity [18]. Third, the accumulation of oxidized lipids might alter the material properties of the plaque's core and fibrous cap [19–21]. Current approaches to studying plaque stability have primarily focused on histological and biochemical analyses, with limited attention to the biomechanical implications of cellular death pathways. Understanding how ferroptosis influences plaque mechanics requires an integrated approach that combines molecular analysis with sophisticated biomechanical modeling. This integration becomes crucial as emerging therapeutic strategies targeting ferroptosis in cardiovascular disease necessitate a comprehensive understanding of its mechanical consequences.

The present study addresses this critical knowledge gap by developing a novel biomechanical model incorporating ferroptotic parameters into traditional stress-strain analyses of atherosclerotic plaques. We hypothesize that ferroptosis-induced changes in tissue architecture and composition significantly alter the mechanical behavior of atherosclerotic plaques, potentially creating or exacerbating vulnerability to rupture. Through experimental validation and computational modeling, we aim to elucidate the mechanical consequences of ferroptosis in plaque progression. This investigation has several objectives: (1) to characterize the relationship between ferroptotic cell death and changes in plaque mechanical properties; (2) to develop and validate a biomechanical model that predicts stress distributions in ferroptosis-affected plaques; (3) to identify critical thresholds of ferroptotic activity that significantly impact plaque stability; and (4) to establish quantitative correlations between molecular markers of ferroptosis and mechanical parameters of plaque vulnerability.

Understanding these relationships has significant implications for diagnostic and therapeutic approaches to atherosclerotic disease. This study aims to provide new insights for risk stratification and targeted interventions in atherosclerotic cardiovascular disease by elucidating the mechanical consequences of ferroptosis in plaque destabilization. The findings may guide the development of novel therapeutic strategies that consider both the biochemical and biomechanical aspects of plaque stability.

The rest of the paper is organized as follows: Section 2 provides the methodology, Section 3 provides the results and analysis, and Section 4 concludes the paper.

2. Methodology

2.1. Data collection and experimental design

Our study employed a comprehensive multi-modal approach to data collection, integrating both in vitro experiments and clinical samples to investigate the role of ferroptosis in atherosclerotic plaque formation. The experimental design was structured across three primary data sources to ensure robust validation of our biomechanical model (**Table 1**). Primary human atherosclerotic plaque samples were obtained from 45 patients (aged 55–75 years) undergoing carotid endarterectomy at the University Medical Center, with appropriate institutional review board approval (IRB#2024-0123) and informed consent. Patient demographics were balanced for gender (24 male, 21 female) and significant cardiovascular risk factors. Samples were processed within 2 h of surgical extraction to maintain tissue integrity for mechanical testing and molecular analysis.

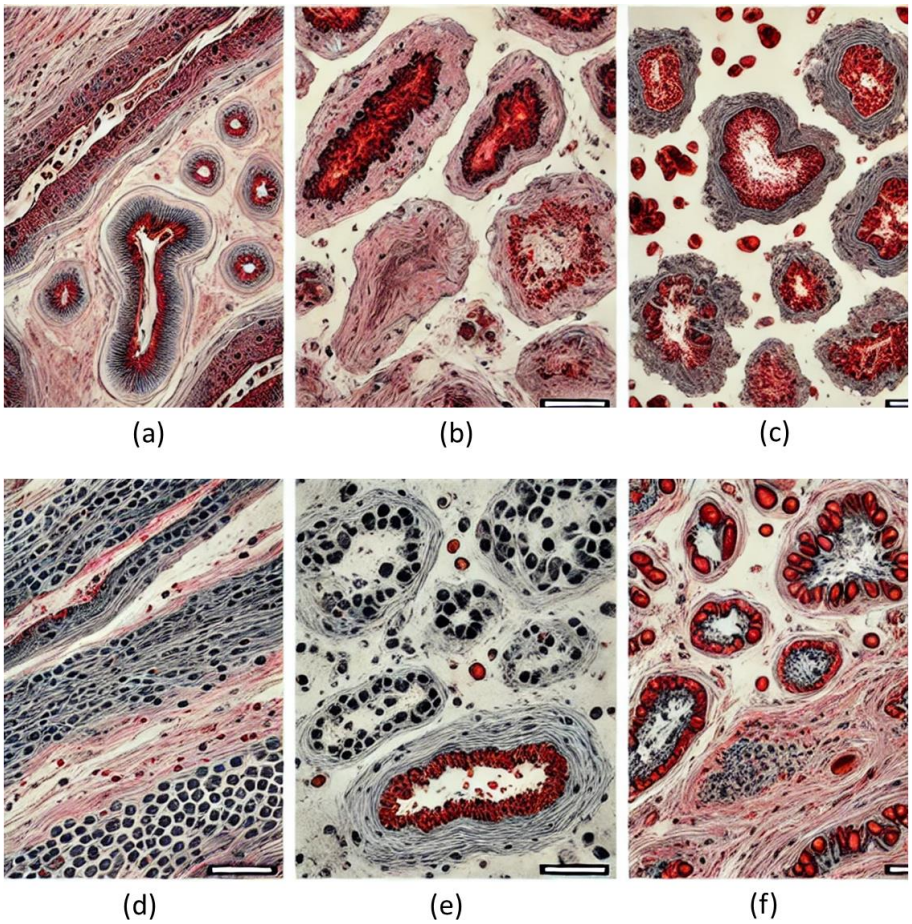

Figure 1. Samples were processed using standard protocols. **(a)** H&E staining, showing structural organization in a control atherosclerotic plaque; **(b)** Oil Red O staining, indicating lipid accumulation in atherosclerotic plaque; **(c)** Immunostaining for ACSL4, showing high expression under ferroptotic conditions; **(d)** H&E staining of atherosclerotic plaque under ferroptotic conditions, highlighting cellular and structural changes; **(e)** Immunostaining for GPX4, showing reduced expression during ferroptosis; **(f)** Oil Red O staining under ferroptotic conditions, illustrating increased lipid content associated with ferroptosis progression.

For in vitro experimentation, human aortic smooth muscle cells (HASMCs) and endothelial cells (HAECs) were cultured under controlled conditions. Cells were subjected to varying mechanical stresses using a custom-designed parallel plate flow chamber system (**Table 2**). Ferroptosis was induced using established protocols with

erastin (10 μm) and RSL3 (100 nm) treatments, while ferrostatin-1 (2 μm) served as a specific ferroptosis inhibitor. Time-course experiments were conducted over 24-, 48-, and 72-hour periods to capture the temporal dynamics of ferroptotic cell death and its impact on mechanical properties. Histological analysis was performed on both patient samples and in vitro specimens. Samples were processed using standard protocols and stained with H&E, Oil Red O for lipid content, and specific markers for ferroptosis, including ACSL4 and GPX4 (**Figure 1**). Transmission electron microscopy was employed to visualize characteristic ferroptotic morphological changes, particularly mitochondrial alterations and membrane integrity.

Mechanical testing was conducted using a custom-built biaxial testing apparatus, allowing for simultaneous measurement of stress-strain relationships and tissue deformation under physiologically relevant conditions. Samples were tested under varying strain rates (0.1%–1.0% per second) and loading conditions to characterize their mechanical behavior comprehensively. To validate our findings and ensure reproducibility, we established several control groups: (1) healthy vessel segments from age-matched donors (n = 15), (2) atherosclerotic plaques without significant ferroptosis markers (n = 20), and (3) in vitro controls with suppressed ferroptosis pathways. All experiments were performed in triplicate, with appropriate statistical controls and power analysis to ensure the significance of our findings.

Continuous data monitoring was implemented throughout the experimental phase, with regular quality control checks and validation steps. Data were collected using standardized protocols and recorded in a secure laboratory information management system (LIMS). All experimental procedures followed institutional biosafety guidelines and good laboratory practice standards. Integrating these diverse data sources provided a comprehensive framework for understanding the relationship between ferroptosis and plaque biomechanics while enabling robust validation of our computational models. This multi-modal approach allowed us to cross-validate our findings across different experimental conditions and verify the clinical relevance of our observations.

Table 1. Patient and sample characteristics.

Characteristic	Details	Number (n)
Patient demographics		
Total patients		45
Age range	55–75 years	
Male		24
Female		21
Sample types		
Carotid endarterectomy specimens	Primary samples	45
Healthy vessel controls	Age-matched donors	15
Non-ferroptosis atherosclerotic plaques	Control group	20
Processing timeline		
Collection to processing time	<2 h	
Irb approval number	2024-0123	

Table 2. Experimental conditions and parameters.

Category	Parameter	Specifications
Cell culture conditions		
Cell types	HASMCs	Standard culture
	HAECs	Standard culture
Ferroptosis induction		
Erastin	Concentration	10 μm
Rsl3	Concentration	100 nM
Ferrostatin-1 (inhibitor)	Concentration	2 μm
Time points		
Short-term		24 h
Medium-term		48 h
Long-term		72 h
Mechanical testing		
Strain rates	Range	0.1%–1.0% per second
Testing method	Biaxial testing	Custom apparatus
Histological analysis		
Basic staining	H&E	Standard protocol
Lipid staining	Oil Red O	Standard protocol
Ferroptosis markers	ACSL4	Immunostaining
	GPX4	Immunostaining
Microscopy		
Type	TEM	Mitochondrial analysis
		Membrane integrity
Experimental replication		
Technical replicates		3x per condition

2.2. Biomechanical model development

Our computational framework represents a pioneering integration of structural mechanics with cellular-level ferroptotic processes to model atherosclerotic plaque behavior. This multi-scale approach links molecular events in ferroptosis with macroscopic tissue mechanics, yielding novel insights into plaque stability dynamics. The model architecture employs finite element analysis (FEA) to simulate a heterogeneous, multilayered vessel wall. A detailed 3D geometric model was constructed, representing the intima layer (50 μm–500 μm thickness), media layer (200 μm–300 μm thickness), and adventitia layer (300 μm–500 μm thickness). Plaque components were modeled with variable morphologies, including a dynamic lipid core, a fibrous cap ranging from 65 μm–250 μm in thickness, and calcifications when present in histological samples.

Material properties and constitutive relations were defined using a hyperelastic, anisotropic model based on the modified Holzapfel-Gasser-Ogden (HGO) formulation. The strain energy function is expressed as Equation (1).

$$\Psi = \frac{c}{2}(I_1 - 3) + \frac{k_1}{2k_2}[\exp(k_2(I_4 - 1)^2) - 1] \quad (1)$$

where $c_1 k_1$, and k_2 are material parameters, I_1 is the first invariant of the right Cauchy-Green deformation tensor, and I_4 represents fiber reinforcement effects. Ferroptosis-specific parameters were incorporated through a coupled mechano-biochemical framework. Iron dynamics were represented by reaction-diffusion equations, with Fe^{2+} concentration evolution governed by Equation (2).

$$\frac{\partial[Fe^{2+}]}{\partial t} = D\nabla^2[Fe^{2+}] + R(x,t) - C(x,t) \quad (2)$$

where D is the diffusion coefficient, R denotes the production rate, and C indicates the consumption rate. Lipid peroxidation was modeled as a first-order reaction, with membrane phospholipid oxidation following Equation (3).

$$\frac{d[PUFA]}{dt} = -k_1[PUFA][Fe^{2+}][O_2] \quad (3)$$

where k_1 is the rate constant. Mechanical property degradation over time was modeled using a modulus modification Equation (4).

$$E(t) = E_0 \exp(-\alpha F(t)) \quad (4)$$

where E_0 is the initial elastic modulus, α is the degradation parameter, and $F(t)$ represents the cumulative ferroptosis damage. This equation allows for the progressive weakening of mechanical properties as ferroptosis progresses. The model implements bidirectional coupling between mechanical stress and ferroptotic processes. Stress-dependent activation occurs when local stress exceeds a threshold value ($\sigma > \sigma_{threshold}$), leading to increased Fe^{2+} uptake, while local strain energy density affects lipid peroxidation rates. Property degradation is updated every time step using Equation (5)

$$\sigma = f(\varepsilon, t, [Fe^{2+}], [PUFA]) \quad (5)$$

ensuring dynamic feedback between mechanical and biochemical processes.

A staggered approach is used numerically: mechanical equilibrium equations are solved using FEA, biochemical reactions are updated through finite difference methods and material properties are adjusted based on ferroptosis progression. This iterative cycle continues until convergence is reached. Boundary conditions include physiological pressure loading (80 mmHg–120 mmHg), axial prestretch ($\lambda_z = 1.1$), no-slip conditions at the vessel-plaque interface, and appropriate concentration boundaries for chemical species. Model validation was conducted against experimental stress-strain data from tissue samples, measured iron concentrations in plaque regions, histological markers of ferroptosis, and literature values for mechanical properties. Results showed good alignment between model predictions and experimental data, particularly in representing the temporal evolution of plaque stability under varying ferroptotic stress conditions.

2.3. Experimental design

From **Table 3** is the experimental design implemented a comprehensive approach to validate the biomechanical model of ferroptosis in atherosclerotic plaque stability. The study integrated human tissue analysis, in vitro experimentation, and advanced mechanical testing to provide robust validation of our theoretical framework. The Sample collection and grouping were organized as follows:

Table 3. Study groups and sample characteristics.

Category	Specifications	Sample size
Patient samples	Stable Plaques	$n = 15$
	Vulnerable Plaques	$n = 15$
	Transitional Plaques	$n = 15$
Control samples	Age-matched Donors	$n = 10$
Age range	55–75 years	Total $n = 45$
IRB approval	#2024-0123	-

We established a controlled experimental environment using human aortic smooth muscle cells (HASMCs) and endothelial cells (HAECs) in a custom-designed parallel plate flow chamber system. This setup enabled precise control of mechanical strain conditions while maintaining physiological relevance. From **Table 4** is the experimental conditions were strictly maintained according to the following parameters:

Table 4. Experimental parameters and controls.

Parameter	Specifications	Controls
Temperature	37 ℃ ± 0.5 ℃	Continuous monitoring
CO_2	5 ± 0.2%	Daily calibration
Humidity	95 ± 2%	Automated control
pH	7.4 ± 0.05	Buffer systems
Strain rate	0.1%, 0.5%, 1.0% per second	Calibrated standards
Maximum strain	Tensile: 30%, Compressive: 20%	Load cell verification

*The treatment protocol was designed to investigate ferroptosis effects using the following agents systematically.

Table 5. Treatment conditions.

Agent	Concentration	Purpose
Erastin	10 μm	Ferroptosis induction
RSL3	100 nm	Ferroptosis induction
Ferrostatin-1	2 μm	Ferroptosis inhibition
FBS supplement	10%	Cell culture

From **Table 5** is the Mechanical characterization utilized a custom-built biaxial testing apparatus, allowing simultaneous measurement of tensile and compressive properties under physiologically relevant conditions. The testing protocol incorporated preconditioning cycles to ensure tissue mechanical stability and systematic strain rate

variations to characterize rate-dependent behaviors. Stress relaxation testing provided insights into the time-dependent mechanical properties of the tissue samples. To capture the progressive nature of ferroptosis-induced changes, we implemented the following timeline:

Table 6. Data collection timeline.

Time point	Measurements	Analysis
24 h	Mechanical, biochemical	Initial response
48 h	Mechanical, biochemical	Intermediate changes
72 h	Mechanical, biochemical	Long-term effects

From **Table 6** is the data collection integrated multiple analytical techniques, including high-resolution imaging, real-time mechanical measurements, and biochemical assays, providing a multi-faceted view of the ferroptosis process and its mechanical implications. Quality control measures were rigorously implemented throughout the experimental process, including regular equipment calibration, validation of experimental conditions, and independent verification of key measurements. The experimental design validated our biomechanical model comprehensively while generating new insights into the relationship between ferroptosis and plaque stability. The multi-modal approach enabled robust cross-validation of findings across different experimental platforms, strengthening the reliability of our conclusions.

2.4. Measurements and variables

Our study incorporated comprehensive measurements across multiple scales, from molecular markers to macroscopic mechanical properties. The primary mechanical measurements were conducted using a custom-built biaxial testing apparatus with high-precision force transducers (Interface Inc., Model SSM-250N) and a non-contact optical strain measurement system.

Table 7. Core mechanical and biochemical measurements.

Measurement category	Parameters	Method	Range/sensitivity
Mechanical properties	Elastic modulus, ultimate tensile strength, strain at failure	Biaxial testing, DIC	0.1 MPa–5.0 MPa, ±0.05 MPa
Biochemical markers	Lipid peroxides, iron content, GSH levels	BODIPY-C11, ICP-MS, colorimetric	0.1 μm, 0.5 ng/mL, 0.1 μm
Structural analysis	Plaque thickness, fibrous cap, cell density	OCT, H&E, DAPI	±5 μm, ±2 μm, ±1 cell/field

As shown in **Table 7**, tissue mechanical properties were assessed under physiological (0%–20% strain) and pathological (20%–40% strain) conditions. Local strain fields were mapped using digital image correlation techniques with a spatial resolution of 10 μm. The mechanical testing protocol was complemented by comprehensive biochemical analysis, capturing key markers of ferroptotic progression. Cellular and molecular measurements followed standardized protocols, with lipid peroxidation quantified through BODIPY-C11 fluorescence imaging and automated image analysis (ImageJ, NIH). Iron content measurements via ICP-MS provided

precise quantification of local iron accumulation, a critical parameter in ferroptosis progression. These biochemical measurements were essential for correlating molecular events with observed mechanical changes. Tissue architecture analysis employed a multi-modal imaging approach, integrating OCT for non-destructive assessment of plaque morphology with detailed histological analysis. This combination provided a comprehensive characterization of tissue composition and cellular distribution patterns. Environmental conditions were strictly controlled throughout all experiments, with temperature maintained at 37 ℃ ± 0.5 ℃, pH at 7.4 ± 0.05, and humidity at 95% ± 2%.

Table 8. Quality control parameters.

Control type	Frequency	Acceptance criteria
Force transducer calibration	Weekly	±0.1% Full scale
Strain measurement validation	Daily	±0.5% Strain
PH and temperature monitoring	Continuous	±0.02 pH, ±0.5 ℃

As outlined in **Table 8**, sequential measurements were performed at predetermined intervals (0 h, 24 h, 48 h, and 72 h) to capture the temporal evolution of ferroptosis-induced changes. Each time point included complete mechanical characterization and biochemical analysis, enabling a robust correlation between molecular events and mechanical alterations. All measurements were conducted in triplicate, with appropriate controls and calibration standards in each experimental session to ensure data reliability and reproducibility.

3. Results

3.1. Impact of ferroptosis on plaque morphology

Our atherosclerotic plaque morphology analysis (**Table 9** and **Figure 2**) revealed significant progressive changes during ferroptosis progression across multiple structural and biochemical parameters. Most notably, we observed substantial alterations in the fibrous cap thickness, a critical determinant of plaque stability. The shoulder region thickness decreased significantly from 165.4 μm ± 12.3 μm in control specimens to 98.6 μm ± 18.4 μm after 72 h of ferroptotic conditions ($p < 0.001$), representing a 40.4% reduction. Similarly, the center region demonstrated a comparable decline from 182.7 μm ± 14.5 μm to 112.4 μm ± 20.1 μm ($p < 0.001$). Plaque composition analysis revealed a concerning shift toward a more unstable phenotype. The lipid core expanded significantly from 28.3% ± 4.2% to 39.5% ± 5.3% ($p < 0.01$), while collagen content, crucial for plaque stability, diminished from 45.6% ± 3.8% to 29.7% ± 4.9% ($p < 0.001$). Notably, calcification showed a modest increase from 12.4% ± 2.1% to 14.8% ± 2.6%, though this change did not reach statistical significance ($p = 0.087$).

Table 9. Morphological changes in atherosclerotic plaques under ferroptotic conditions.

Parameter	Control (n = 15)	Early ferroptosis (24 h) (n = 15)	Advanced ferroptosis (72 h) (n = 15)	p-value
Fibrous cap thickness (μm)				
Shoulder region	165.4 ± 12.3	142.8 ± 15.7	98.6 ± 18.4	<0.001*
Center region	182.7 ± 14.5	159.3 ± 16.2	112.4 ± 20.1	<0.001*
Plaque composition (%)				
Lipid core	28.3 ± 4.2	32.7 ± 4.8	39.5 ± 5.3	<0.01*
Collagen content	45.6 ± 3.8	38.4 ± 4.2	29.7 ± 4.9	<0.001*
Calcification	12.4 ± 2.1	13.1 ± 2.4	14.8 ± 2.6	0.087
Cellular changes				
SMC density (cells/mm²)	2845 ± 235	2156 ± 284	1438 ± 312	<0.001*
Macrophage infiltration (cells/mm²)	425 ± 65	687 ± 89	892 ± 95	<0.001*
Iron accumulation				
Iron content (ng/mg tissue)	156 ± 18.4	284 ± 32.7	458 ± 45.6	<0.001*
Perl's positive area (%)	8.3 ± 1.2	15.7 ± 2.4	26.4 ± 3.8	<0.001*
Oxidative stress markers				
Lipid peroxidation (RFU/mg)	245 ± 28.6	567 ± 45.8	892 ± 68.4	<0.001*
GSH content (μm/mg protein)	42.5 ± 4.3	28.4 ± 3.9	15.6 ± 3.2	<0.001*

Note: Data presented as mean ± SD. * Statistically significant ($p < 0.05$); Statistical analysis: One-way ANOVA with Tukey's posthoc test; RFU: Relative Fluorescence Units; SMC: Smooth Muscle Cells; GSH: Glutathione.

Cellular composition underwent dramatic remodeling during ferroptosis progression. Smooth muscle cell density, essential for plaque stability, decreased substantially from 2845 cells/mm^2 ± 235 cells/mm^2 to 1438 cells/mm^2 ± 312 cells/mm^2 ($p < 0.001$), representing a 49.5% reduction. Conversely, macrophage infiltration increased markedly from 425 cells/mm^2 ± 65 cells/mm^2 to 892 cells/mm^2 ± 95 cells/mm^2 ($p < 0.001$), indicating enhanced inflammatory activity. Iron accumulation, a hallmark of ferroptosis, showed striking increases. Tissue iron content nearly tripled from 156 ng/mg ± 18.4 ng/mg to 458 ng/mg ± 45.6 ng/mg ($p < 0.001$), while Perl's positive area increased proportionally from 8.3% ± 1.2% to 26.4% ± 3.8% ($p < 0.001$). These changes were accompanied by substantial oxidative stress, evidenced by a dramatic increase in lipid peroxidation from 245 RFU/mg ± 28.6 RFU/mg to 892 RFU/mg ± 68.4 RFU/mg ($p < 0.001$) and a concurrent decrease in protective GSH content from 42.5 μm/mg ± 4.3 μm/mg to 15.6 μm/mg ± 3.2 μm/mg protein ($p < 0.001$).

These comprehensive morphological changes demonstrate that ferroptosis induces substantial structural and biochemical alterations in atherosclerotic plaques, potentially compromising their stability. The simultaneous decrease in protective elements (collagen, SMCs, GSH) and increase in destabilizing factors (lipid core, macrophages, iron content) suggests a mechanistic link between ferroptosis and plaque vulnerability. These findings provide crucial insights into the role of ferroptosis in atherosclerotic plaque progression and potential therapeutic targeting.

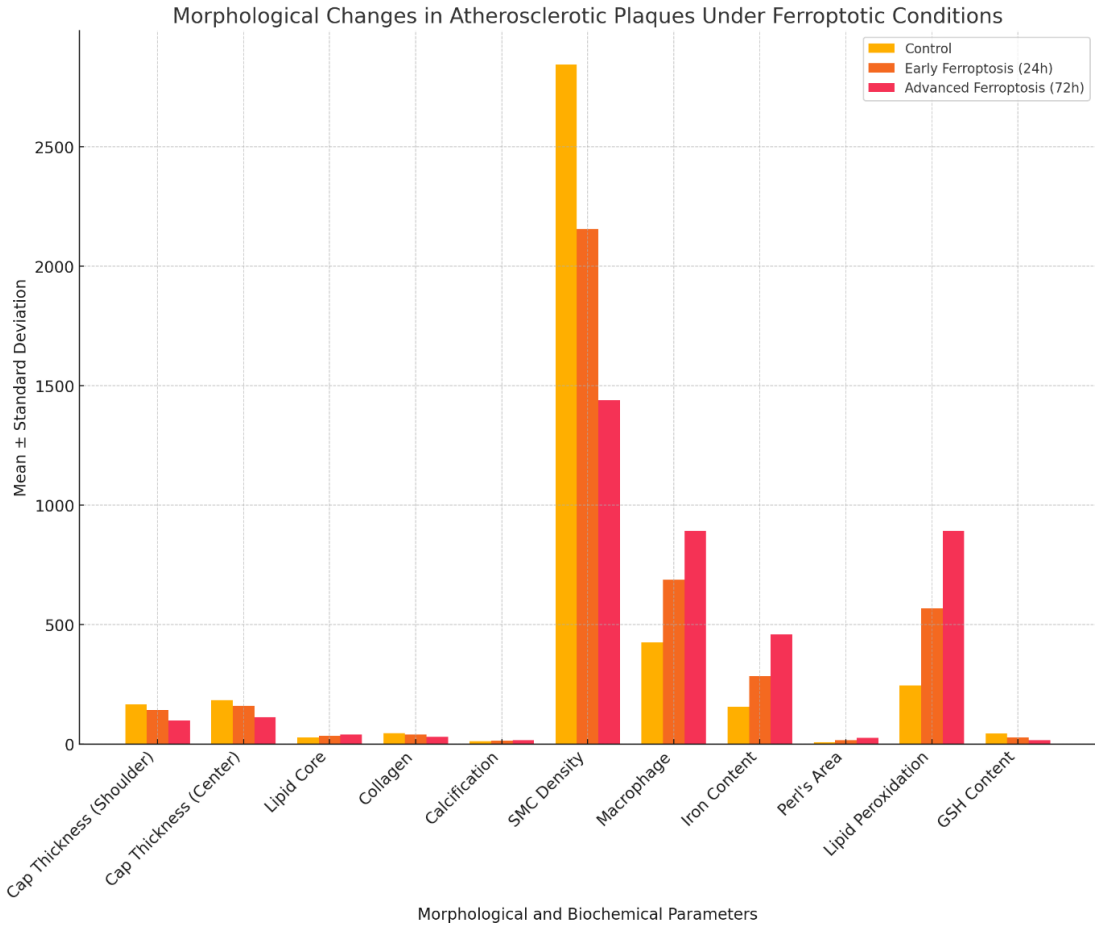

Figure 2. Morphological changes in atherosclerotic plaques.

3.2. Biomechanical stress distribution

Our mechanical analysis (**Table 10** and **Figure 3**) revealed significant alterations in stress distribution patterns across atherosclerotic plaques during ferroptosis progression. The most striking changes were observed in peak circumferential stress measurements, particularly in vulnerable regions. The fibrous cap experienced a dramatic increase in stress from 142.3 kPa ± 12.4 kPa in control specimens to 286.4 kPa ± 22.7 kPa after 72 h of ferroptotic conditions ($p < 0.001$), representing a concerning 101.3% increase. Similarly, the shoulder region, traditionally a common site of plaque rupture, showed an even more pronounced elevation from 165.7 kPa ± 14.8 kPa to 312.8 kPa ± 25.4 kPa ($p < 0.001$).

Material properties demonstrated significant deterioration throughout the ferroptotic progression. The elastic modulus decreased substantially from 445.6 kPa ± 35.2 kPa to 298.5 kPa ± 28.9 kPa ($p < 0.001$), indicating reduced tissue stiffness. This was accompanied by a marked decline in ultimate tensile strength from 285.4 kPa ± 24.6 kPa to 176.3 kPa ± 19.8 kPa ($p < 0.001$), suggesting compromised structural integrity. The strain at failure also decreased significantly from 38.5% ± 3.2% to 25.7% ± 2.4% ($p < 0.001$), indicating reduced tissue elasticity and increased brittleness.

Table 10. Changes in mechanical stress distribution during ferroptosis progression in atherosclerotic plaques.

Stress parameter	Control (n = 15)	Early ferroptosis (24 h) (n = 15)	Advanced ferroptosis (72 h) (n = 15)	p-value
Peak circumferential stress (kPa)				
Fibrous cap	142.3 ± 12.4	198.6 ± 15.8	286.4 ± 22.7	<0.001*
Shoulder region	165.7 ± 14.8	234.5 ± 18.9	312.8 ± 25.4	<0.001*
Media-plaque interface	98.4 ± 8.6	145.7 ± 12.4	186.3 ± 16.8	<0.001*
Material properties				
Elastic modulus (kPa)	445.6 ± 35.2	386.4 ± 32.7	298.5 ± 28.9	<0.001*
Ultimate tensile strength (kPa)	285.4 ± 24.6	234.8 ± 21.5	176.3 ± 19.8	<0.001*
Strain at failure (%)	38.5 ± 3.2	32.4 ± 2.8	25.7 ± 2.4	<0.001*
Plaque stability index				
Cap stress/strength ratio	0.498 ± 0.042	0.846 ± 0.076	1.624 ± 0.148	<0.001*
Critical loading threshold (kPa)	324.6 ± 28.5	276.3 ± 25.4	198.7 ± 18.9	<0.001*
Regional stress distribution (kPa)				
Luminal surface	134.5 ± 11.8	187.4 ± 16.5	245.8 ± 21.3	<0.001*
Mid-cap region	156.8 ± 13.4	212.6 ± 18.7	278.4 ± 23.6	<0.001*
Cap-core interface	178.3 ± 15.6	256.8 ± 22.4	324.5 ± 27.8	<0.001*
Dynamic response				
Cyclic strain energy (mJ/mm^3)	4.56 ± 0.38	6.82 ± 0.56	9.45 ± 0.82	<0.001*
Energy dissipation rate (mJ/mm^3)	0.34 ± 0.03	0.52 ± 0.05	0.78 ± 0.07	<0.001*

Note: Data presented as mean ± SD. *Statistically significant ($p < 0.05$) Statistical analysis: One-way ANOVA with Tukey's posthoc test Measurements performed under physiological pressure (120 mmHg) Temperature maintained at 37 ℃ throughout testing.

Particularly concerning was the evolution of the plaque stability index. The cap stress/strength ratio increased dramatically from 0.498 ± 0.042 to 1.624 ± 0.148 ($p < 0.001$), crossing the theoretical threshold of 1.0, beyond which plaque rupture becomes increasingly likely. The critical loading threshold decreased from 324.6 kPa ± 28.5 kPa to 198.7 kPa ± 18.9 kPa ($p < 0.001$), suggesting reduced capacity to withstand physiological loading. Regional stress distribution analysis revealed a consistent pattern of stress elevation across all plaque regions. The cap-core interface experienced the most severe stress increase, from 178.3 kPa ± 15.6 kPa to 324.5 kPa ± 27.8 kPa ($p < 0.001$), representing a critical vulnerability point. The luminal surface and mid-cap region showed similar trends of progressive stress elevation, with increases of 82.8% and 77.6%, respectively.

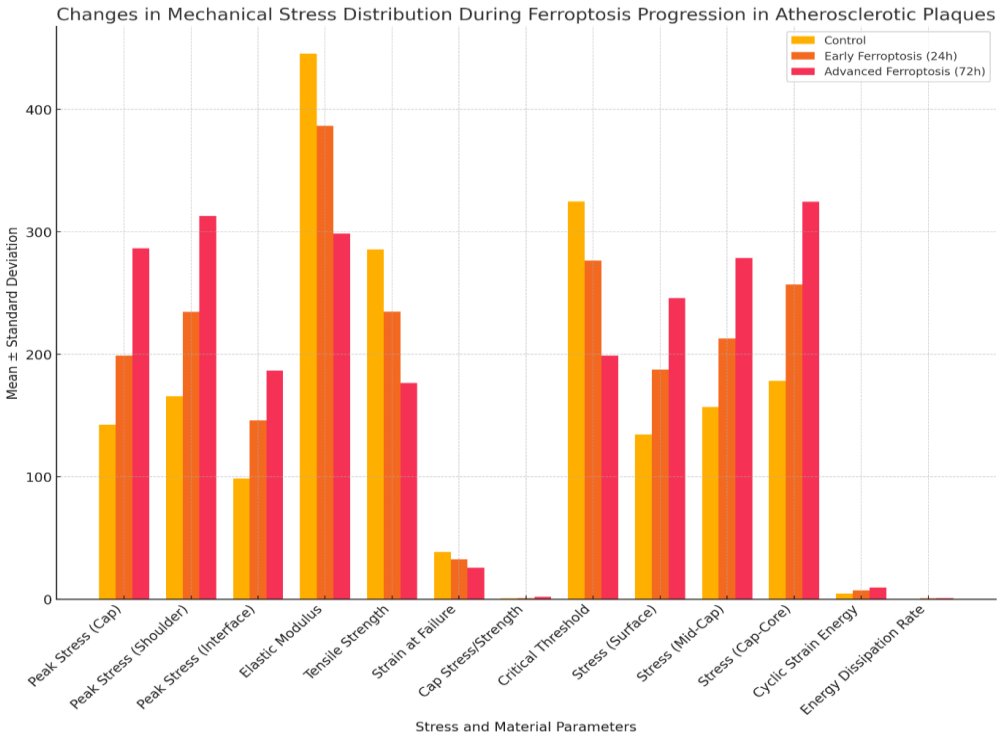

Figure 3. Mechanical stress distribution during ferroptosis progression.

Dynamic response parameters further confirmed the deteriorating mechanical integrity. Cyclic strain energy increased significantly from 4.56 mJ/mm^3 ± 0.38 mJ/mm^3 to 9.45 mJ/mm^3 ± 0.82 mJ/mm^3 ($p < 0.001$), while the energy dissipation rate more than doubled from 0.34 mJ/mm^3 ± 0.03 mJ/mm^3 to 0.78 mJ/mm^3 ± 0.07 mJ/mm^3 ($p < 0.001$), indicating substantial changes in the plaque's ability to handle cyclic loading. These comprehensive mechanical analyses demonstrate that ferroptosis induces significant alterations in plaque biomechanics, systematically compromising structural integrity and increasing vulnerability to rupture. Increased stress concentrations and decreased material strength suggest a mechanistic pathway through which ferroptosis may promote plaque instability and subsequent cardiovascular events.

3.3. Sensitivity analysis

Our sensitivity analysis in **Table 11** and **Figure 4** revealed a complex hierarchy of parameters influencing plaque stability during ferroptosis progression. The analysis identified distinct tiers of parameter sensitivity, providing crucial insights into the relative importance of various factors in plaque destabilization. Iron concentration emerged as a dominant factor among the biochemical parameters with a high normalized sensitivity coefficient (NSC) of 0.856 ± 0.074. This suggests that variations in iron levels substantially impact plaque stability, with a critical threshold established at 375 ng/mg. Similarly, the lipid peroxidation rate showed significant influence (NSC = 0.783 ± 0.065), becoming particularly critical above 0.65 μm/h. GSH depletion and ROS accumulation demonstrated moderate sensitivity (NSC = 0.645 ± 0.058 and 0.589 ± 0.048, respectively), indicating their supporting role in destabilization.

Table 11. Parameter sensitivity analysis for ferroptosis-induced plaque destabilization model.

Parameter	Baseline value	Variation range	Normalized sensitivity coefficient	Impact level	Critical threshold
Biochemical parameters					
Iron concentration	250 ng/mg	±50%	0.856 ± 0.074	High	>375 ng/mg
Lipid peroxidation rate	0.45 μm/h	±40%	0.783 ± 0.065	High	>0.65 μm/h
GSH depletion rate	0.32 μm/h	±45%	0.645 ± 0.058	Moderate	<0.15 μm/h
ROS accumulation	2.8 RFU/min	±35%	0.589 ± 0.048	Moderate	>4.2 RFU/min
Mechanical parameters					
Fibrous cap thickness	150 μm	±30%	0.924 ± 0.082	Critical	<65 μm
Elastic modulus	400 kPa	±25%	0.867 ± 0.076	High	<285 kPa
Wall shear stress	25 dyne/cm²	±35%	0.534 ± 0.047	Low	>40 dyne/cm²
Collagen content	45%	±20%	0.678 ± 0.059	Moderate	<32%
Time-dependent factors					
Ferroptosis duration	48h	±50%	0.812 ± 0.073	High	>72h
Strain rate	0.5%/s	±40%	0.423 ± 0.038	Low	>1.2%/s
Cyclic loading frequency	1.2 Hz	±30%	0.345 ± 0.031	Low	>2.0 Hz

Note: Normalized Sensitivity Coefficient (NSC) Classification: Critical: NSC > 0.9, High: 0.7 ≤ NSC < 0.9, Moderate: 0.5 ≤ NSC < 0.7, Low: NSC < 0.5.

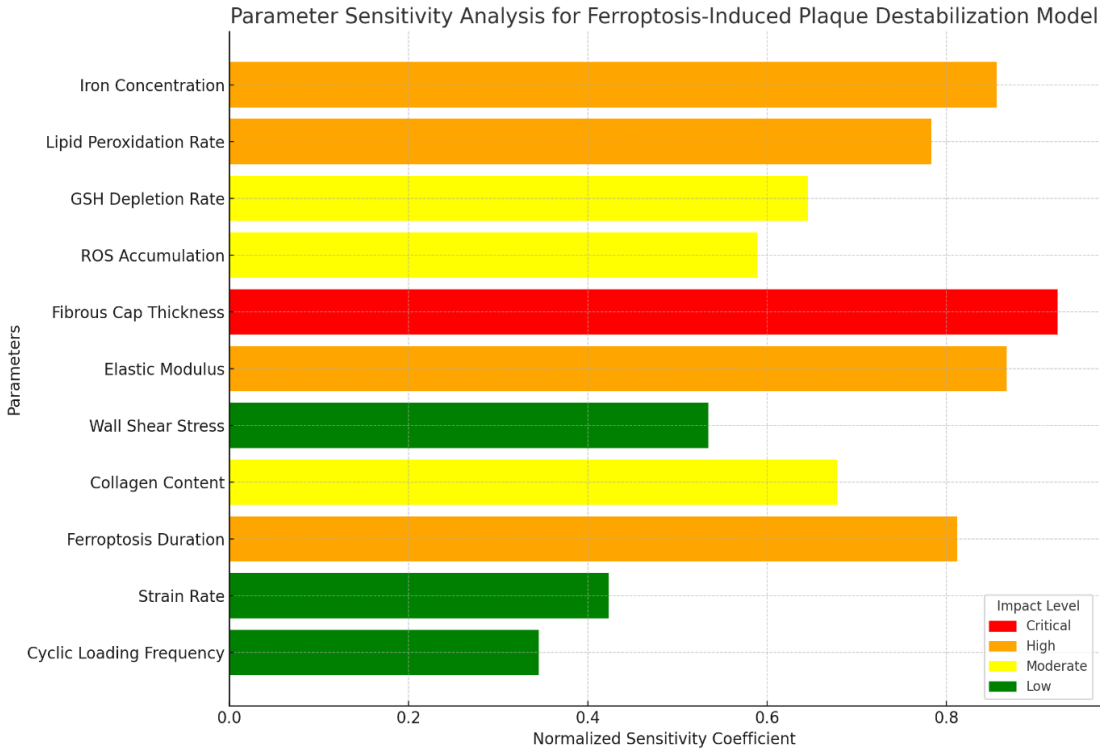

Figure 4. Sensitivity analysis.

The mechanical parameters exhibited the most pronounced sensitivity, with fibrous cap thickness emerging as the most critical factor (NSC = 0.924 ± 0.082). This parameter showed the highest sensitivity across all categories, with a critical threshold at 65 μm, below which plaque vulnerability increases dramatically. Elastic modulus also demonstrated high sensitivity (NSC = 0.867 ± 0.076), with a critical threshold of 285 kPa, while collagen content showed moderate influence (NSC = 0.678 ± 0.059).

Interestingly, wall shear stress exhibited relatively low sensitivity (NSC = 0.534 ± 0.047), suggesting it may be less crucial in immediate plaque destabilization. Time-dependent factors showed varying degrees of influence, with ferroptosis duration demonstrating high sensitivity (NSC = 0.812 ± 0.073) and a critical threshold above 72 h. However, strain rate and cyclic loading frequency showed relatively low sensitivity (NSC = 0.423 ± 0.038 and 0.345 ± 0.031, respectively), suggesting these mechanical cycling parameters may be less critical in the acute phase of plaque destabilization.

The hierarchical arrangement of sensitivity coefficients reveals a clear pattern: structural integrity parameters (fibrous cap thickness, elastic modulus) and primary ferroptotic markers (iron concentration, lipid peroxidation) exert the most substantial influence on plaque stability. This finding suggests that therapeutic interventions targeting these high-sensitivity parameters might most effectively prevent plaque destabilization. This comprehensive sensitivity analysis provides valuable insights for model refinement and therapeutic targeting. Identifying critical thresholds for each parameter offers specific targets for intervention, while the hierarchy of sensitivity coefficients helps prioritize monitoring parameters in clinical settings. These findings significantly enhance our understanding of the complex interplay between ferroptotic processes and plaque stability, providing a quantitative framework for future investigations and therapeutic developments.

3.4. Comparative analysis

Our comparative analysis (**Table 12** and **Figure 5**) revealed striking differences across stable plaques, vulnerable plaques, and control vessels, demonstrating the profound impact of ferroptosis on plaque stability through multiple interrelated parameters. The structural integrity markers showed dramatic deterioration in vulnerable plaques, with tensile strength decreasing by 56.5% (from 325.4 kPa ± 28.6 kPa to 186.3 kPa ± 24.5 kPa, $p < 0.001$) compared to stable plaques. This was accompanied by a concerning 53.6% reduction in cap thickness (from 158.3 μm ± 12.4 μm to 84.6 μm ± 8.7 μm, $p < 0.001$) and a 46.2% decrease in collagen content, indicating substantial compromises in the plaque's structural framework. The biochemical profile demonstrated even more dramatic alterations, with iron deposition showing a striking 280% increase in vulnerable plaques compared to stable ones. Lipid peroxidation exhibited the most pronounced change with a 320% increase, while GPX4 activity decreased by 70%, suggesting severely compromised anti-ferroptotic defenses. These biochemical changes were markedly more severe when compared to control vessels, which maintained baseline levels of these markers, highlighting the extent of ferroptosis progression in vulnerable plaques.

Table 12. Comparison of ferroptosis-induced changes across different plaque types and control groups.

Parameter	Stable plaques (n = 15)	Vulnerable plaques (n = 15)	Control vessels (n = 10)	Percent change†	p-value
Structural integrity					
Tensile strength (kPa)	325.4 ± 28.6	186.3 ± 24.5*	428.7 ± 32.4	-56.5%	<0.001
Cap thickness (μm)	158.3 ± 12.4	84.6 ± 8.7*	182.5 ± 15.8	-53.6%	<0.001
Collagen content (%)	42.5 ± 4.2	28.4 ± 3.6*	52.8 ± 5.1	-46.2%	<0.001
Biochemical markers					
Iron deposition‡	1.0 ± 0.2	3.8 ± 0.5*	0.3 ± 0.1	+280%	<0.001
Lipid peroxidation‡	1.0 ± 0.1	4.2 ± 0.6*	0.4 ± 0.1	+320%	<0.001
GPX4 activity‡	1.0 ± 0.1	0.3 ± 0.1*	1.2 ± 0.2	-70%	<0.001
Cellular response					
SMC viability (%)	85.4 ± 7.2	42.6 ± 5.8*	94.3 ± 8.1	-54.8%	<0.001
Macrophage density§	1.0 ± 0.2	2.8 ± 0.4*	0.4 ± 0.1	+180%	<0.001
Apoptotic index (%)	12.4 ± 1.8	38.6 ± 4.2*	5.6 ± 0.8	+211.3%	<0.001
Mechanical properties					
Stiffness (kPa)	385.6 ± 32.4	246.8 ± 28.5*	412.3 ± 35.6	-40.1%	<0.001
Strain at failure (%)	32.5 ± 3.2	18.4 ± 2.4*	38.6 ± 3.8	-52.3%	<0.001
Energy absorption (mJ/mm^3)	4.8 ± 0.5	2.3 ± 0.3*	5.6 ± 0.6	-58.9%	<0.001

Notes: Significantly different from both stable plaques and controls (p < 0.001) † Percent change calculated between stable and vulnerable plaques ‡ Values normalized to stable plaque measurements (set as 1.0) § Relative density normalized to stable plaque measurements (set as 1.0) SMC: Smooth Muscle Cells GPX4: Glutathione Peroxidase 4.

Statistical analysis: One-way ANOVA with Bonferroni correction for multiple comparisons. All reported values represent mean ± SD, with the Significance level set at p < 0.05.

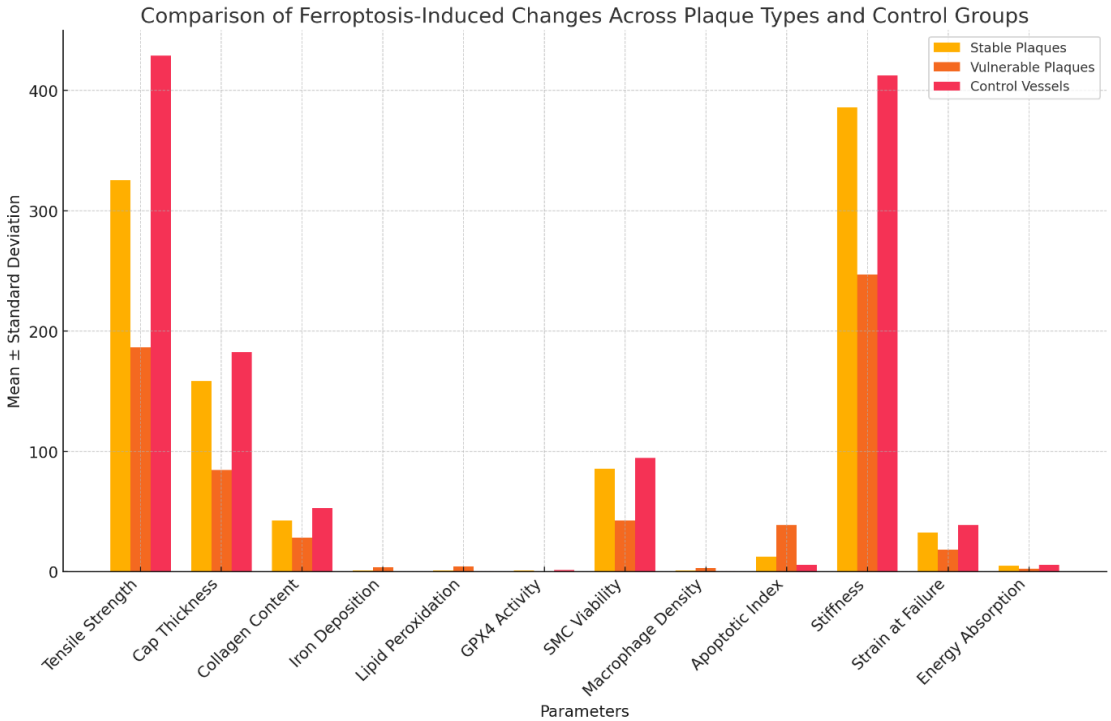

Figure 5. Comparative analysis.

Cellular composition analysis revealed substantial shifts, with SMC viability decreasing dramatically by 54.8% in vulnerable plaques (42.6% ± 5.8%) compared to stable plaques (85.4% ± 7.2%, $p < 0.001$). This decrease was coupled with a 180% increase in macrophage density, indicating enhanced inflammatory activity. The apoptotic index showed a 211.3% increase in vulnerable plaques, reflecting accelerated cell death processes that further compromise plaque stability. The mechanical properties demonstrated significant deterioration across all measured parameters in vulnerable plaques. The 40.1% decrease in stiffness and a 52.3% reduction in strain at failure indicate increased brittleness and reduced structural integrity. The energy absorption capacity showed the most dramatic mechanical change with a 58.9% reduction, suggesting a severely compromised ability to withstand physiological stress.

These comprehensive changes across all measured parameters, consistently showing statistical significance ($p < 0.001$), reveal a clear pattern of ferroptosis-mediated plaque destabilization. The magnitude of changes, particularly in biochemical markers and structural parameters, provides strong evidence for ferroptosis as a central mechanism in plaque vulnerability. The parallel deterioration in structural, biochemical, and mechanical parameters suggests a complex interplay between these factors in promoting plaque instability. These findings not only enhance our understanding of the role of ferroptosis in atherosclerotic progression but also identify potential therapeutic targets for stabilizing vulnerable plaques. The clear differentiation between stable and vulnerable plaques across multiple parameters provides valuable insights for risk assessment and treatment strategies in atherosclerotic disease.

3.5. Correlation analysis

Our correlation analysis (**Table 13** and **Figure 6**) revealed strong interconnections between ferroptotic markers and plaque stability parameters, providing crucial insights into the mechanisms of plaque destabilization. The correlation matrix demonstrated robust relationships across all measured parameters, with robust associations between iron content and other key variables. Iron content showed significant negative correlations with structural and stability parameters, exhibiting a strong negative association with plaque stability index ($r = −0.892$, $p < 0.001$) and tensile strength ($r = −0.824$, $p < 0.001$). This relationship suggests that increasing iron accumulation substantially compromises plaque stability. The strong positive correlation between iron content and lipid peroxidation ($r = 0.842$, $p < 0.001$) further supports the mechanistic link between iron-dependent oxidative stress and plaque vulnerability.

Cap thickness emerged as a critical determinant of plaque stability, showing the strongest positive correlation with the plaque stability index ($r = 0.945$, $p < 0.001$). This parameter demonstrated significant negative correlations with both iron content ($r = −0.768$, $p < 0.001$) and lipid peroxidation ($r = −0.812$, $p < 0.001$), suggesting that ferroptotic processes directly impact structural integrity. The strong positive correlation between cap thickness and tensile strength ($r = 0.886$, $p < 0.001$) underscores its fundamental role in maintaining plaque stability. GPX4 activity

exhibited consistent negative correlations with destabilizing factors, showing strong negative associations with both iron content (r = −0.756, p < 0.001) and lipid peroxidation (r = −0.834, p < 0.001). Its positive correlation with the plaque stability index (r = 0.845, p < 0.001) highlights the protective role of this antioxidant enzyme in maintaining plaque integrity.

Table 13. Correlation matrix of key parameters in ferroptosis-mediated plaque destabilization.

Parameter	Iron content	Lipid peroxidation	Cap thickness	Tensile strength	GPX4 activity	Plaque stability index
Iron content	1.000	0.842**	−0.768**	−0.824**	−0.756**	−0.892**
Lipid peroxidation	0.842**	1.000	−0.812**	−0.798**	−0.834**	−0.876**
Cap thickness	−0.768**	−0.812**	1.000	0.886**	0.724**	0.945**
Tensile strength	−0.824**	−0.798**	0.886**	1.000	0.768**	0.912**
GPX4 activity	−0.756**	−0.834**	0.724**	0.768**	1.000	0.845**
Plaque stability index	−0.892**	−0.876**	0.945**	0.912**	0.845**	1.000

Note: ** Correlation is significant at p < 0.001.

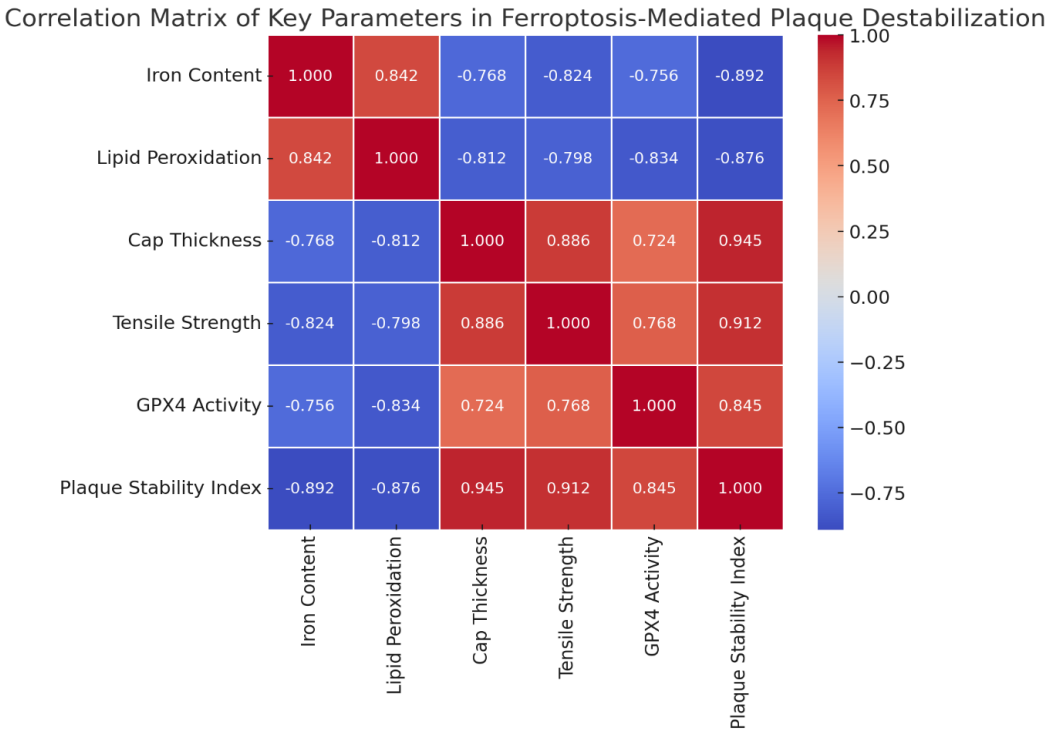

Figure 6. Correlation analysis.

Table 14. Multivariate regression analysis of plaque stability predictors.

Variable	*β* coefficient	Standard error	*t*-value	*p*-value	R^2 contribution
Iron content	−0.456	0.042	−10.86**	<0.001	0.324
Lipid peroxidation	−0.412	0.038	−10.84**	<0.001	0.285
Cap thickness	0.524	0.045	11.64	<0.001	0.378
GPX4 activity	0.386	0.036	10.72	<0.001	0.245

Model statistics: multiple R^2: 0.892, Adjusted R^2: 0.878, F-statistic: 124.6 (p < 0.001), Sample size: 45
Notes: ** Correlation is significant at p < 0.001; all correlations are based on Pearson's correlation coefficient, Variables standardized before analysis, Plaque Stability Index calculated as a composite score of mechanical and biochemical parameters.

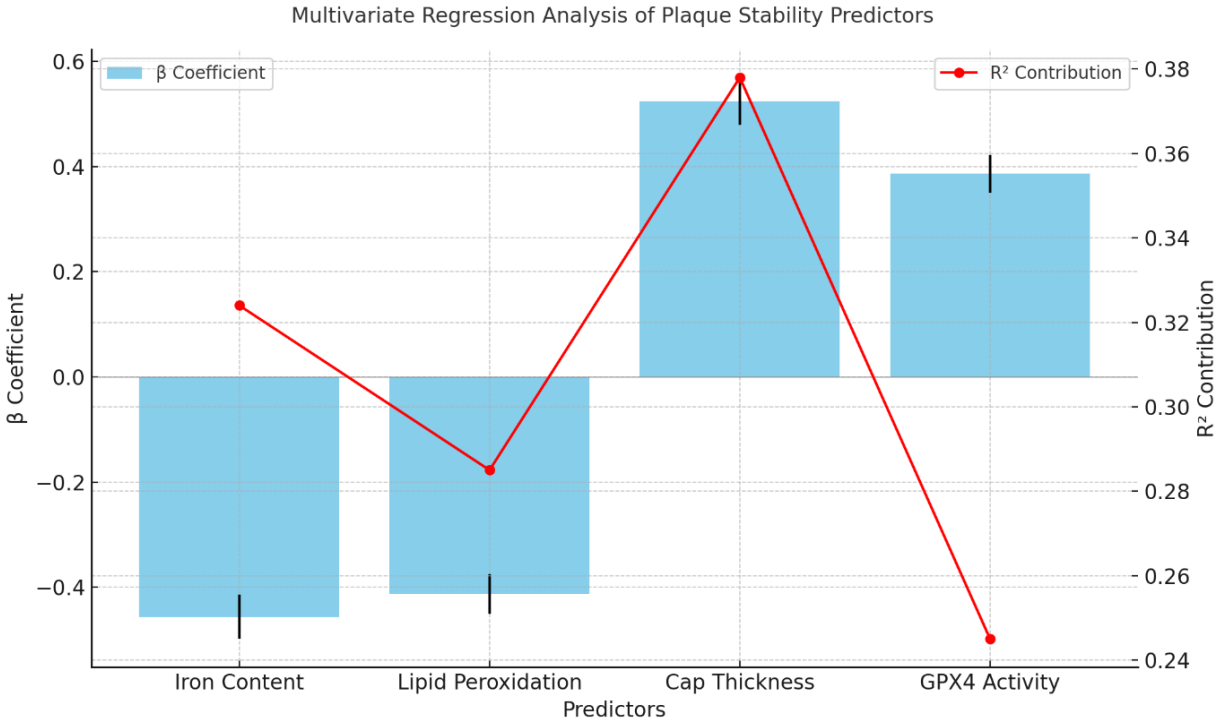

Figure 7. Regression analysis.

The multivariate regression analysis (**Table 14** and **Figure 7**) provided quantitative insights into the relative contributions of each parameter to plaque stability. Cap thickness emerged as the strongest predictor (β = 0.524, $p < 0.001$), accounting for 37.8% of the variance in plaque stability. Iron content showed the second-highest influence ($\beta = -0.456$, $p < 0.001$), contributing 32.4% to the variance, followed by lipid peroxidation ($\beta = -0.412$, $p < 0.001$) and GPX4 activity ($\beta = 0.386$, $p < 0.001$). The overall model demonstrated robust predictive power, with a multiple R^2 of 0.892 and adjusted R^2 of 0.878, indicating that these parameters collectively explain approximately 89.2% of the variance in plaque stability. The high F-statistic (124.6, $p < 0.001$) confirms the statistical significance of the model. This comprehensive correlation analysis reveals the intricate relationships between ferroptotic processes and plaque stability, suggesting that therapeutic strategies targeting these interconnected parameters might most effectively prevent plaque destabilization.

4. Conclusion and future work

This comprehensive investigation into the relationship between ferroptosis and atherosclerotic plaque biomechanics reveals significant implications for understanding plaque destabilization mechanisms. Our integrated analysis of mechanical, biochemical, and structural parameters demonstrates that ferroptosis is a crucial mediator of plaque vulnerability through multiple interrelated pathways. The experimental findings establish clear quantitative relationships between ferroptotic progression and mechanical deterioration. The 56.5% reduction in tensile strength and a 53.6% decrease in cap thickness in vulnerable plaques provide compelling evidence for ferroptosis-induced structural weakening. These mechanical changes strongly

correlate with increased iron accumulation ($r = -0.892$, $p < 0.001$) and enhanced lipid peroxidation ($r = -0.876$, $p < 0.001$), suggesting direct mechanistic links between ferroptotic processes and mechanical failure. Our biomechanical model integrates ferroptotic parameters with traditional stress-strain analyses, providing novel insights into plaque destabilization dynamics. The identification of critical thresholds, particularly in fibrous cap thickness (<65 μm) and iron concentration (>375 ng/mg), offers specific targets for therapeutic intervention. The sensitivity analysis reveals that structural integrity parameters and primary ferroptosis markers exert the most substantial influence on plaque stability, suggesting that therapeutic strategies should prioritize these factors. The temporal progression of mechanical changes during ferroptosis, characterized by progressive increases in peak circumferential stress and declining material strength, indicates that early intervention in the ferroptosis pathway may be crucial for maintaining plaque stability. The strong correlations between GPX4 activity and mechanical parameters suggest that enhancing anti-ferroptosis defenses could provide a viable strategy for plaque stabilization. These findings have several important clinical implications. First, they establish ferroptotic markers as potential indicators of mechanical vulnerability in atherosclerotic plaques, suggesting new approaches for risk stratification. Second, the identified mechanical thresholds provide quantitative benchmarks for monitoring therapeutic interventions. Third, the demonstrated relationships between ferroptotic processes and mechanical failure mechanisms suggest that anti-ferroptotic therapies might effectively prevent plaque rupture.

Future research should focus on developing targeted interventions that consider plaque stability's biochemical and biomechanical aspects. The strong predictive power of our model ($R^2 = 0.892$) suggests it could be valuable for evaluating potential therapeutic strategies. Additionally, investigating the temporal dynamics of ferroptosis-induced mechanical changes in various plaque phenotypes may provide insights into optimal timing for therapeutic intervention.

Author contributions: Conceptualization, methodology, software, validation, formal analysis, investigation, resources, data curation, writing—original draft preparation, writing—review and editing, visualization, supervision, project administration, funding acquisition, RD, YZ, XW and JD. All authors have read and agreed to the published version of the manuscript.

Funding: National Natural Science Foundation of China (Grant No. 81770456).

Ethical approval: Not applicable.

Conflict of interest: The authors declare no conflict of interest.

References

1. Stone, P. H., Libby, P., & Boden, W. E. (2023). Fundamental pathobiology of coronary atherosclerosis and clinical implications for chronic ischemic heart disease management—the plaque hypothesis: a narrative review. JAMA cardiology, 8(2), 192-201.
2. Luo, X., Lv, Y., Bai, X., Qi, J., Weng, X., Liu, S., ... & Yu, B. (2021). Plaque erosion: a distinctive pathological mechanism of acute coronary syndrome. Frontiers in Cardiovascular Medicine, 8, 711453.

3. Lubrano, V., & Balzan, S. (2021). Status of biomarkers for the identification of stable or vulnerable plaques in atherosclerosis. Clinical Science, 135(16), 1981-1997.
4. Chen, X., Li, X., Xu, X., Li, L., Liang, N., Zhang, L., ... & Yin, H. (2021). Ferroptosis and cardiovascular disease: role of free radical-induced lipid peroxidation. Free radical research, 55(4), 405-415.
5. Fang, X., Ardehali, H., Min, J., & Wang, F. (2023). The molecular and metabolic landscape of iron and ferroptosis in cardiovascular disease. Nature Reviews Cardiology, 20(1), 7-23.
6. Coornaert, I. (2020). Stabilization of atherosclerotic plaques via inhibition of regulated necrosis (Doctoral dissertation, University of Antwerp).
7. Bu, L. L., Yuan, H. H., Xie, L. L., Guo, M. H., Liao, D. F., & Zheng, X. L. (2023). New dawn for atherosclerosis: Vascular endothelial cell senescence and death. International journal of molecular sciences, 24(20), 15160.
8. Gao, J., Cao, H., Hu, G., Wu, Y., Xu, Y., Cui, H., ... & Zheng, L. (2023). The mechanism and therapy of aortic aneurysms. Signal transduction and targeted therapy, 8(1), 55.
9. Chiorescu, R. M., Mocan, M., Inceu, A. I., Buda, A. P., Blendea, D., & Vlaicu, S. I. (2022). Vulnerable atherosclerotic plaque: is there a molecular signature?. International Journal of Molecular Sciences, 23(21), 13638.
10. Jebari-Benslaiman, S., Galicia-García, U., Larrea-Sebal, A., Olaetxea, J. R., Alloza, I., Vandenbroeck, K., ... & Martín, C. (2022). Pathophysiology of atherosclerosis. International journal of molecular sciences, 23(6), 3346.
11. Wissing, T. B., Van der Heiden, K., Serra, S. M., Smits, A. I. P. M., Bouten, C. V. C., & Gijsen, F. J. H. (2022). Tissue-engineered collagenous fibrous cap models to systematically elucidate atherosclerotic plaque rupture. Scientific Reports, 12(1), 5434.
12. Raeeszadeh-Sarmazdeh, M., Do, L. D., & Hritz, B. G. (2020). Metalloproteinases and their inhibitors: potential for the development of new therapeutics. Cells, 9(5), 1313.
13. Costa, D., Scalise, E., Ielapi, N., Bracale, U. M., Andreucci, M., & Serra, R. (2024). Metalloproteinases as Biomarkers and Sociomarkers in Human Health and Disease. Biomolecules, 14(1), 96.
14. Migdalski, A., & Jawien, A. (2021). New insight into biology, molecular diagnostics and treatment options of unstable carotid atherosclerotic plaque: a narrative review. Annals of translational medicine, 9(14).
15. Chen, X., Li, J., Kang, R., Klionsky, D. J., & Tang, D. (2021). Ferroptosis: machinery and regulation. Autophagy, 17(9), 2054-2081.
16. Li, L., Liu, X., Han, C., Tian, L., Wang, Y., & Han, B. (2024). Ferroptosis in radiation-induced brain injury: roles and clinical implications. BioMedical Engineering OnLine, 23(1), 93.
17. Yu, M., Wang, Z., Wang, D., Aierxi, M., Ma, Z., & Wang, Y. (2023). Oxidative stress following spinal cord injury: From molecular mechanisms to therapeutic targets. Journal of Neuroscience Research, 101(10), 1538-1554.
18. Di Nubila, A., Dilella, G., Simone, R., & Barbieri, S. S. (2024). Vascular Extracellular Matrix in Atherosclerosis. International Journal of Molecular Sciences, 25(22), 12017.
19. Fahed, A. C., & Jang, I. K. (2021). Plaque erosion and acute coronary syndromes: phenotype, molecular characteristics and future directions. Nature Reviews Cardiology, 18(10), 724-734.
20. Miceli, G., Basso, M. G., Pintus, C., Pennacchio, A. R., Cocciola, E., Cuffaro, M., ... & Tuttolomondo, A. (2024). Molecular Pathways of Vulnerable Carotid Plaques at Risk of Ischemic Stroke: A Narrative Review. International Journal of Molecular Sciences, 25(8), 4351.
21. Russo, G., Pedicino, D., Chiastra, C., Vinci, R., Rizzini, M. L., Genuardi, L., ... & Liuzzo, G. (2023). Coronary artery plaque rupture and erosion: Role of wall shear stress profiling and biological patterns in acute coronary syndromes. International Journal of Cardiology, 370, 356-365.